Multiscale Relaxation Dynamics in Ultrathin Metallic Glass-Forming Films

Q. L. Bi,[1] Y. J. Lü,[1,*] and W. H. Wang[2]
[1]School of Physics, Beijing Institute of Technology, Beijing 100081, People's Republic of China
[2]Institute of Physics, Chinese Academy of Sciences, Beijing 100190, People's Republic of China

(Received 24 September 2017; revised manuscript received 26 December 2017; published 9 April 2018)

The density layering phenomenon originating from a free surface gives rise to the layerlike dynamics and stress heterogeneity in ultrathin Cu-Zr glassy films, which facilitates the occurrence of multistep relaxations in the timescale of computer simulations. Taking advantage of this condition, we trace the relaxation decoupling and evolution with temperature simply via the intermediate scattering function. We show that the β relaxation hierarchically follows fast and slow modes in films, and there is a β-relaxation transition as the film is cooled close to the glass transition. We provide the direct observation of particle motions responsible for the β relaxation and reveal the dominant mechanism varying from the thermal activated to the cooperative jumps across the transition.

DOI: 10.1103/PhysRevLett.120.155501

Relaxation phenomena of supercooled liquids and glasses have been paid special attention due to the crucial role in understanding the nature of the glass transition and glassy state [1–4]. On approaching the glass transition temperature T_g, the dynamics of supercooled liquids is slowed down accompanied by the multiscale relaxation of density fluctuations. The structural relaxation (α) responsible for the glass transition manifests a super-Arrhenius increase in time. Behind the α relaxation, a short-time secondary relaxation, named Johari-Goldstein β relaxation, has been observed in supercooled liquids and structural glasses [5–7]. The β relaxation has been argued to be governed by stringlike clusters of particles with a cooperative motion [8,9]. The two relaxation processes merge near the dynamical crossover to the mode coupling behavior [10,11]. With a decreasing temperature down to the glassy state, the β relaxation becomes dominant, which is closely related to the plastic deformation of metallic glasses [12,13]. However, growing experimental evidence suggests that the relaxation behavior in a glassy state is more complicated than a simple β process. The dielectric spectroscopy measurements in organic glasses have shown that the temperature dependence of the β relaxation tends to decline when cooled into the glassy state [14–16]. The mechanical analysis on a La-based metallic glass has reported the existence of a fast additional β relaxation in a low-temperature region [17]. A more intriguing phenomenon is the findings of the underlying relaxation decoupling in glassy solids: The enthalpy recovery of the well-aged glassy polymers has been found to exhibit two-step behavior during equilibration, implying the presence of two timescales of relaxation [18]. This decoupling is supported by the recent stress decay analysis in bulk metallic glasses [19]. The new secondary relaxation features the compressed exponential shape of density correlation functions and is believed to result from ballisticlike motion driven by the internal stress in nonequilibrium states [20,21].

The surface of a metallic glass (MG) shows significantly high mobility, and the diffusion has been proved to even be 10^5 times the bulk value [22–24]. Enhanced mobility makes the surface relaxation more sufficient in the experimental timescale, thus beneficial for fabricating the ultrastable glass by vapor deposition [25,26]. When the system is reduced to a very small size, the surface effect increasingly dominates. Low-dimensional MGs are thus expected to exhibit unusual relaxation behaviors. In this Letter, we report the multiscale relaxations in ultrathin MG films by using molecular dynamics (MD) simulations. We find that the strong density layering associated with the surface produces wavelike fluctuations of dynamics and stress which facilitate multimode relaxations in the simulation timescale.

The $Cu_{50}Zr_{50}$ films were chosen as the model to investigate the relaxation dynamics. A slab system ($L_x = L_y =$ 76 Å) is sandwiched by two vacuum cells along the $\pm z$ directions and then is relaxed at $T = 1800$ K to form a well-equilibrated liquid film. We prepared the samples with the thicknesses ranging from $12a$ to $3a$ ($a = 4.224$ Å, the lattice constant of a Cu-Zr compound). The cavitation occurs as $d < 3a$. These films were quenched to 500 K in the constant volume and temperature ensemble (NVT). Crystallization never occurs under the present simulation conditions. The calorimetric T_g is determined by the temperature behavior of enthalpy, depending on the film thickness [27]. The following discussion focuses on the temperature range of $T_g \pm 200$ K. The single-particle dynamics method was used to interpret the microscopic mechanism of multiple relaxations [31,32]. Further details of the MD simulation are provided in Supplemental Material [27].

For bulk MGs, the secondary β-relaxation process has never been clearly observed in the time dependence of static correlation functions due to weak signatures. Alternately, the mechanical response functions are frequently used to explore the existence of β relaxation in a glassy state, and the behavior in a supercooled region is accordingly obtained by extrapolation. We find that, as the thickness of films is reduced to a very small size ($d < 6a$), the secondary relaxation processes are sensitively detected in the intermediate scattering function (ISF) normal to the surface, which is given by

$$F_{s,z}(q,t) = \frac{1}{N_0}\sum_{j=1}^{N_0}\langle \exp\{i\mathbf{q}\cdot[\mathbf{r}_{j,z}(0) - \mathbf{r}_{j,z}(t)]\}\rangle, \quad (1)$$

where N_0 denotes the atomic number and $\mathbf{r}_{j,z}$ is the position of atom j along the z direction (normal to the surface). The wave vector q is 2.688 Å^{-1}, corresponding to the location of the first peak in the structure factor. Figure 1 shows the normal ISFs for $d = 3a$ at different temperatures around the glass transition ($T_g \approx 620$ K). At small supercoolings, $F_{s,z}(q,t)$ decays to zero exponentially within 1 ps. When liquids are cooled below 1200 K, a departure from the exponential decay appears. The single nonexponential decay evolves into a two-step decay close to 800 K, as shown in Fig. 1. In fact, we find that the first decay consists of two substeps separated by an inflection point in the correlator. To clearly identify the locations of points, we consider the logarithmic derivatives of ISF $\Delta(t) \equiv d[\log(F_{s,z})]/d[\log(t)]$; representative plots of $\Delta(t)$ are given in the inset in Fig. 1. Three distinct maxima at $t_1 \approx 0.3$, $t_2 \approx 1.5$, and $t_3 \approx 7.5$ ps separate four regimes, which persists throughout the glass transition. At very short times ($t < t_1$), the ISF shows a fast drop, corresponding to the ballistic regime. The long-time decay in the last regime ($t > t_3$) represents the α relaxation. We classify the other two short-time decays ($t_1 < t < t_2$ and $t_2 < t < t_3$) as the subprocesses of the secondary β relaxation. These decay regimes are well fitted to the Kohlrausch-William-Watts (KWW) function, $\phi(t) = A\exp[-(t/\tau)^{\gamma}]$, respectively, where τ is the relaxation time and γ is the exponent [33]. Figure 2(a) shows the temperature dependence of the fitted relaxation times. The single-mode relaxation time follows an Arrhenius increase. With a further decreasing temperature, the relaxation is decoupled into multistep modes with different temperature dependences. The timescale of the primary α relaxation τ_α grows with the Vogel-Fulcher-Tamman (VFT) law; the two sub-β relaxations show the Arrhenius behavior. We define the two subprocesses as the fast and slow β relaxations corresponding to the first and second decay regimes in ISFs. They appear in pairs after the relaxation decoupling in contrast to analogous observations only in the low-temperature glassy state [17]. Upon approaching the glass transition, the temperature variation of the two subrelaxations consistently shows a rapid drop, even approximating temperature independence. This change underlies a transition in microscopic β-relaxation mechanism. Here we empirically locate a transition temperature T_β, for example, $T_\beta = 1.08T_g$ for the film of $d = 3a$ shown in Fig. 2(a), and then divide the β relaxation into two regimes: high-temperature (HT) and low-temperature (LT) β relaxation. The fast (slow) β relaxation is accordingly subdivided into HT and LT fast (slow) β relaxations.

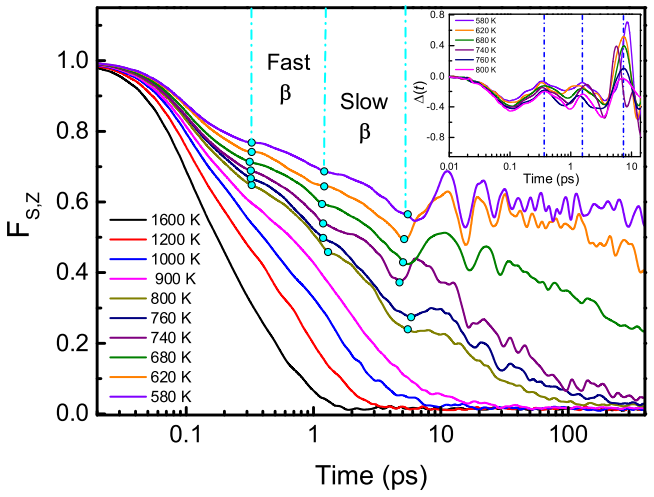

FIG. 1. Intermediate scattering functions as a function of the time for the film with $d = 3a$ at different temperatures. The dots and the dashed lines highlight the secondary β-relaxation regimes including fast and slow subprocesses. The inset presents a plot of the logarithmic derivative of ISFs.

Figure 2(b) shows the exponents fitted to the KWW function for the two subrelaxations. At high T, the exponent $\gamma < 1$ and increases to the compressed regime ($\gamma > 1$) with a decreasing temperature till an approximate constant $\gamma = 1.5$ is reached. Within the temperature range we studied, no significant difference in γ is found between the fast and slow branches. The activation energies for the HT and LT β relaxations, which are fitted to the Arrhenius law separately, are $\Delta E = 0.29 \pm 0.02$ and 0.03 ± 0.02 eV, respectively, regardless of fast and slow modes. These values are smaller than the empirical data of β relaxation for bulk MGs (1–1.5 eV) [34]; in particular, the LT β relaxation shows many weak thermal activation characteristics. The observation of multistep relaxations is influenced by the film thickness. With an increasing thickness, the relaxation times have an overall rise, and the transition to the LT β relaxation shifts to the lower-temperature region [27]. For the films of $d > 5a$, these secondary relaxations cannot been clearly identified in the decay of $F_{s,z}(q,t)$, exhibiting bulk behavior instead.

The multistep relaxation in ultrathin films is further identified in the mean-square displacement (MSD). Figure 3(a) shows a typical MSD normal to the surface close to T_g. After the initial ballistic regime ($t < 0.1$ ps), two cage regimes occur before reaching the diffusive motion.

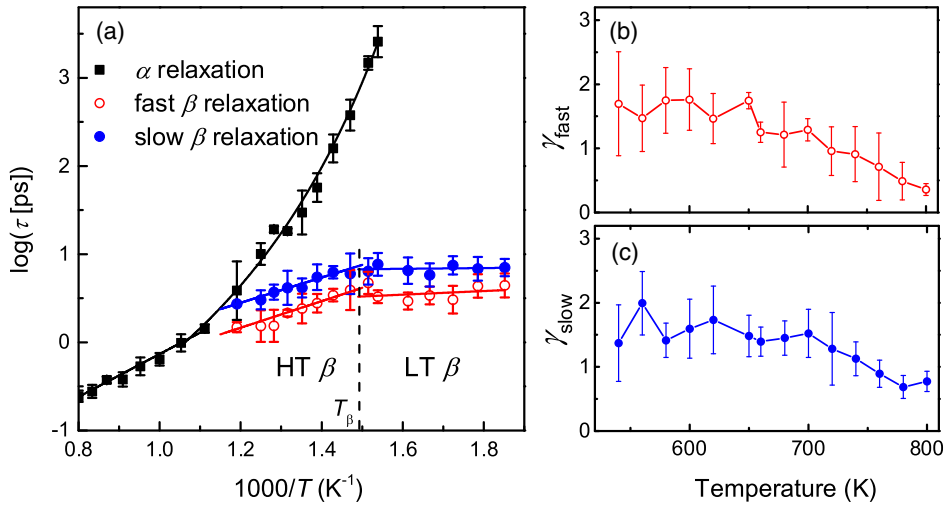

FIG. 2. Relaxation dynamics in $Cu_{50}Zr_{50}$ films. (a) The relaxation time as a function of the reciprocal temperature for $d = 3a$. The solid lines for the fast and the slow β relaxation are fits to the Arrhenius law, and the line for the α relaxation is a fit to the VFT law. (b) and (c) show the exponents fitted to the KWW relation for the fast and slow β relaxations.

The two regimes well correspond to the β and α relaxation regimes in ISF, although the fast and slow modes cannot be distinguished distinctly in MSD. The coincidence indicates that the symbiosis behavior of the α and β relaxations can be described as a cascade of relaxing cages with different sizes. A cage is relaxed by the jump motion, which is confirmed by the time-resolved squared displacements of individual particles [27]. Based on MSDs, we introduce two lengths, l_α and l_β, which correspond to the two inflection points in the MSD curve, to separate the α and the β relaxation. If the jump length l is larger than l_α, the jump is identified as a move involved in α relaxation (named an α jump); if $l_\beta < l < l_\alpha$, it is the β jump for β relaxation. To check the criterion, we calculate jump rates for α and β relaxation, which is defined as the fraction of the jump number N_{jump} per unit observation time t_s, $\upsilon = N_{\text{jump}}/N_0 t_s$. Figure 3(b) shows that α- and β-jump rates decouple as the behavior of the relaxation time. The β-jump rate is approximately temperature invariant after an Arrhenius-type decrease, in contrast to the VFT-type drop of the α-jump rate. These behaviors are consistent with the temperature dependence of reciprocal relaxation times, which, in turn, validate the choice of the two characteristic lengths.

Using this criterion, the motion of individual particles contributing to the β relaxation can be directly identified without any empirical setting. We measure the spatial correlation of β jumps by using a scaled correlation function, $f(r,t) = \mu_j(r,t)/\langle\rho(r)\rangle\mu_0$, where $\mu_j(r,t)$ is the average β-jump density at a distance r for the time t given that the jth β jump is at the origin and $\langle\rho(r)\rangle$ is the average

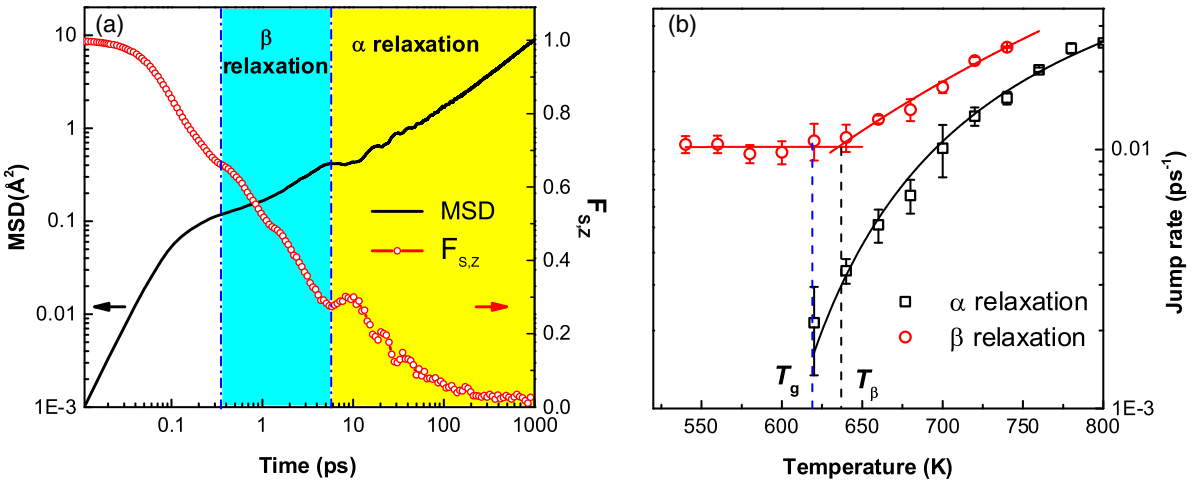

FIG. 3. Jump dynamics featuring multistep relaxations. (a) Mean-square displacement normal to the surface as a function of the time for the $Cu_{50}Zr_{50}$ film with $d = 3a$ and at $T = 700$ K. (b) Jump rates associated with the α and β relaxations as a function of the temperature. The solid lines for the β relaxations are the fits to the Arrhenius law, and that for the α relaxation is the fit to the VFT law.

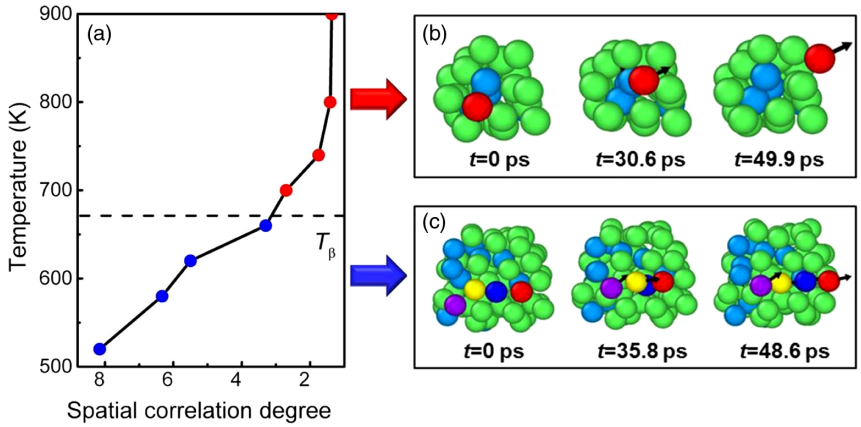

FIG. 4. The jump motion involved in the β relaxation. (a) Spatial correlation degree of jumps as a function of the temperature. (b) An atom (red ball) jumps out of the cage region, which is contributed to the HT β relaxation. (c) A cooperative stringlike jump in the LT β relaxation process. The red, blue, yellow, and purple balls denote the atoms in a string. The light blue and green balls denote the mobile and shell atoms, respectively.

number density of atoms at r (see Supplemental Material [27] for details). We define a spatial correlation degree of jumps, $\chi = \int_0^{r_0} F(r)dr$, where $F(r)$ is the time window average of $f(r,t)$ and r_0 is the average nearest distance between two jumping atoms. Figure 4(a) shows that the spatial correlation of jump motions is considerably enhanced as it is cooled below T_β. The LT β relaxation is reasonably interpreted as the behavior dominated by correlated or cooperative jump motions microscopically, which evolves from the thermally activated random jumps responsible for the HT β relaxation. Figure 4(b) illustrates a typical jump in the HT β relaxation (see Video 1 in Supplemental Material [27]). The jump behaves as an individual event without a pronounced correlation to other jumps. Figure 4(c) displays a jump involved in the LT β relaxation. Like the HT β relaxation, the jump occurs in the highly mobile regions, but differently it proceeds in a cooperative manner with its neighbors. These cooperative jumps join together to form a stringlike configuration [27]. Such cooperative stringlike motion is very similar to cooperatively rearranging regions observed in many supercooled Lennard-Jones [35,36], colloids [37] and metallic liquids [38].

The present multiscale relaxation is closely related to the density layering in ultrathin MG films. In many liquid drops and films, the density profile along the direction normal to the free surface shows a layering behavior [39,40]. The density layering becomes stronger on cooling and ultimately disappears when crystallization occurs [41]. However, the layering is found to survive in glassy films. For $Cu_{50}Zr_{50}$ films, a distinct surface density layering is identified in the samples of $d \leq 10a$ and rapidly decays towards the interior. With a decreasing thickness, the layering is strongly enhanced in magnitude and width. When the thickness is smaller than $5a$, the density layering has penetrated through the film. Figure 5(a) shows the density profiles normal to the surface with different thicknesses at 600 K (this temperature is below T_g for all the films). The presence of the density layering in glassy films is attributed to the fast dynamics of the glassy surface. A high-mobility glassy surface looks like various liquids, thereby preserving the layering feature below T_g. Here a primary concern is whether the observed multiscale relaxation is an artificial result due to averaging over layers with different relaxation dynamics in the calculations. We have calculated ISFs in different layers of the $d = 3a$ film; the relaxation processes in the surface and internal layers show similar multistep modes and timescales [27]. Furthermore, in thicker films with only 1–2 surface layers, for example, $d = 10a$, we have confirmed the presence of multistep relaxation in the surface layer but bulk behavior internally [27]. It is clear that the multiscale relaxation behavior observed in this work faithfully features the intrinsic relaxation dynamics of ultrathin films, and it is also for the surface relaxation dynamics of thicker films.

The strong density layering gives rise to dynamics and stress layering. We use a parameter $k_j(t)$ to measure the dynamic activity of individual particles, $k_j(t) = \sum_{t=0}^{t_{\rm obs}} |\mathbf{r}_j(t+\Delta t) - \mathbf{r}_j(t)|^2\rangle$, which sums the atomic trajectory over the observation time $t_{\rm obs}$, where Δt is the incremental time. Figure 5(b) plots the snapshot of the dynamic activity in configuration space for $d = 3a$ at $T = 600$ K. A layering of mobility forms along the normal direction, coupled with the density layering. Another effect that arises from the density layering is stress layering. Figure 5(c) shows that the tensile and compressive stress regions alternatively distribute. These layering phenomena lead to strong spatial heterogeneities of density, dynamics, and stress. The enhanced dynamic heterogeneity promotes the distinct identification of the secondary relaxations in $F_{s,z}(q,t)$, even the subtle fast and slow subprocesses. The internal stress heterogeneity may be the main reason for the LT β relaxation, as suggested by recent

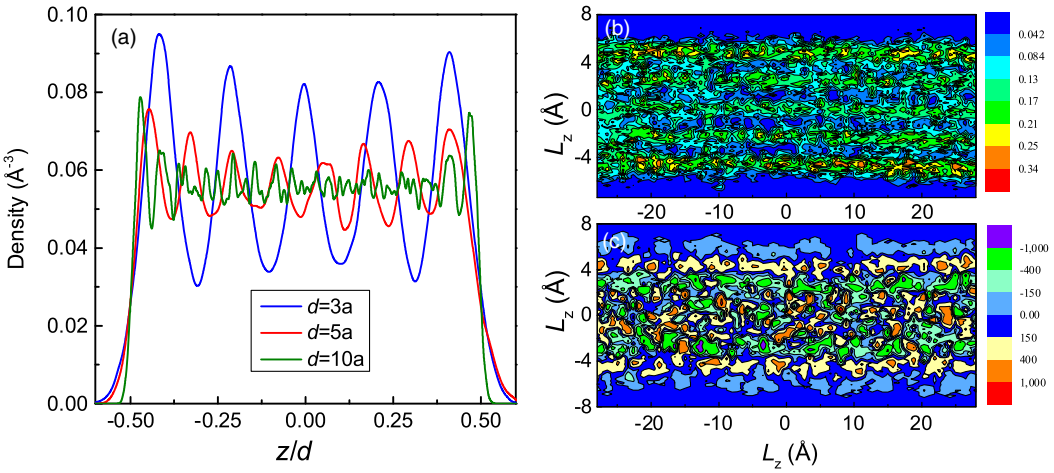

FIG. 5. Density, dynamics, and stress layering. (a) Density profiles of $Cu_{50}Zr_{50}$ films along the z direction with different thicknesses at 600 K. Contour maps of the dynamic activity (b) and normal stress (c) in configuration space.

theoretical work [20,21]. It is noted that the inhomogeneity induced by layering does not exist in the direction parallel to the surface. The tangential α relaxation in the surface layer is found to be quite faster than the bulk one [27], which is the intrinsic mechanism for preparing the ultrastable thin-film glass proposed by Ediger and co-workers [25,26].

In summary, the relaxation dynamics in $Cu_{50}Zr_{50}$ ultrathin films is studied from the supercooling liquid to the glassy state. The density layering phenomenon associated with a free surface gives rise to the significant dynamics and stress heterogeneity in space, which accounts for unusual multistep relaxations across the glass transition. The decoupling of the α and β relaxation is distinctly identified in the time decay of the ISF normal to the surface. On approaching the glass transition, there is a transition from the HT to the LT β relaxation. We find that the secondary β relaxation is universally composed of the fast and slow subprocesses. Microscopically, the HT β relaxation is ascribed to the thermally activated jump motions, and the LT β relaxation is dominated by the cooperative and stringlike jump motions. The ultrathin glassy film provides an ideal model to explore the multiscale relaxation processes in the timescale of molecular simulations and improves our understanding of complicated relaxation phenomena in low-dimensional glassy materials.

This work was supported by the National Natural Science Foundation of China under Contract No. 51171027. The computer resources at the Shanghai and Tianjin Supercomputer Center are gratefully acknowledged.

*yongjunlv@bit.edu.cn

[1] K. L. Ngai, *Relaxation and Diffusion in Complex Systems* (Springer, New York, 2011).
[2] M. D. Ediger, C. A. Angell, and S. R. Nagel, J. Phys. Chem. **100**, 13200 (1996).
[3] C. A. Angell, K. L. Ngai, G. B. McKenna, P. F. McMillan, and S. W. Martin, J. Appl. Phys. **88**, 3113 (2000).
[4] J. C. Dyre, Rev. Mod. Phys. **78**, 953 (2006).
[5] K. L. Ngai and M. Paluch, J. Chem. Phys. **120**, 857 (2004).
[6] H. B. Yu, W. H. Wang, and K. Samwer, Mater. Today **16**, 183 (2013).
[7] P. G. Debenedetti and F. H. Stillinger, Nature (London) **410**, 259 (2001).
[8] J. D. Stevenson and P. G. Wolynes, Nat. Phys. **6**, 62 (2010).
[9] S. Karmakar, C. Dasgupta, and S. Sastry, Phys. Rev. Lett. **116**, 085701 (2016).
[10] W. Götze and L. Sjögren, Rep. Prog. Phys. **55**, 241 (1992).
[11] L. Berthier and G. Biroli, Rev. Mod. Phys. **83**, 587 (2011).
[12] H. B. Yu, X. Shen, Z. Wang, L. Gu, W. H. Wang, and H. Y. Bai, Phys. Rev. Lett. **108**, 015504 (2012).
[13] W. H. Wang, J. Appl. Phys. **110**, 053521 (2011).
[14] N. B. Olsen, T. Christensen, and J. C. Dyre, Phys. Rev. E **62**, 4435 (2000).
[15] M. Paluch, C. M. Roland, S. Pawlus, J. Zioło, and K. L. Ngai, Phys. Rev. Lett. **91**, 115701 (2003).
[16] Z. Fakhraai and J. A. Forrest, Science **319**, 600 (2008).
[17] Q. Wang, S. T. Zhang, Y. Yang, Y. D. Dong, C. T. Liu, and J. Lu, Nat. Commun. **6**, 7876 (2015).
[18] D. Cangialosi, V. M. Boucher, A. Alegría, and J. Colmenero, Phys. Rev. Lett. **111**, 095701 (2013).
[19] P. Luo, P. Wen, H. Y. Bai, B. Ruta, and W. H. Wang, Phys. Rev. Lett. **118**, 225901 (2017).
[20] B. Ruta, G. Baldi, G. Monaco, and Y. Chushkin, J. Chem. Phys. **138**, 054508 (2013).
[21] V. M. Giordano and B. Ruta, Nat. Commun. **7**, 10344 (2016).
[22] Y. Chai, T. Salez, J. D. McGraw, M. Benzaquen, K. Dalnoki-Veress, E. Raphaël, and J. A. Forrest, Science **343**, 994 (2014).
[23] L. Chen, C. R. Cao, J. A. Shi, Z. Lu, Y. T. Sun, P. Luo, L. Gu, H. Y. Bai, M. X. Pan, and W. H. Wang, Phys. Rev. Lett. **118**, 016101 (2017).
[24] C. R. Cao, Y. M. Lu, H. Y. Bai, and W. H. Wang, Appl. Phys. Lett. **107**, 141606 (2015).

[25] S. F. Swallen, K. L. Kearns, M. K. Mapes, S. K. Yong, R. J. Mcmahon, M. D. Ediger, T. Wu, L. Yu, and S. Satija, Science **315**, 353 (2007).
[26] S. Singh, M. D. Ediger, and J. J. de Pablo, Nat. Mater. **12**, 139 (2013).
[27] See Supplemental Material at http://link.aps.org/supplemental/10.1103/PhysRevLett.120.155501 for the technical details about the simulations, videos, and more supplemental figures, which includes Refs. [28–31].
[28] M. Mendelev, M. Kramer, R. Ott, D. Sordelet, D. Yagodin, and P. Popel, Philos. Mag. **89**, 967 (2009).
[29] S. Nosé, J. Chem. Phys. **81**, 511 (1984).
[30] W. G. Hoover, Phys. Rev. A **31**, 1695 (1985).
[31] Y. J. Lü and W. H. Wang, Phys. Rev. E **94**, 062611 (2016).
[32] J. Helfferich, F. Ziebert, S. Frey, H. Meyer, J. Farago, A. Blumen, and J. Baschnagel, Phys. Rev. E **89**, 042603 (2014).
[33] M. D. Ediger, Annu. Rev. Phys. Chem. **51**, 99 (2000).
[34] H. B. Yu, W. H. Wang, H. Y. Bai, Y. Wu, and M. W. Chen, Phys. Rev. B **81**, 220201 (2010).
[35] C. Donati, J. F. Douglas, W. Kob, S. J. Plimpton, P. H. Poole, and S. C. Glotzer, Phys. Rev. Lett. **80**, 2338 (1998).
[36] J. D. Stevenson, J. Schmalian, and P. G. Wolynes, Nat. Phys. **2**, 268 (2006).
[37] E. R. Weeks, J. C. Crocker, A. C. Levitt, A. Schofield, and D. A. Weitz, Science **287**, 627 (2000).
[38] A. Jaiswal, S. OKeeffe, R. Mills, A. Podlesynak, G. Ehlers, W. Dmowski, K. Lokshin, J. Stevick, T. Egami, and Y. Zhang, J. Phys. Chem. B **120**, 1142 (2016).
[39] O. G. Shpyrko, A. Y. Grigoriev, C. Steimer, P. S. Pershan, B. Lin, M. Meron, T. Graber, J. Gerbhardt, B. Ocko, and M. Deutsch, Phys. Rev. B **70**, 224206 (2004).
[40] H. Mo, G. Evmenenko, S. Kewalramani, K. Kim, S. N. Ehrlich, and P. Dutta, Phys. Rev. Lett. **96**, 096107 (2006).
[41] Y. J. Lü, Q. L. Bi, and X. Q. Yan, J. Chem. Phys. **144**, 234508 (2016).